IOP Publishing

Journal of Optics

J. Opt. **24** (2022) 055601 (7pp)

https://doi.org/10.1088/2040-8986/ac5dd4

Multi-value phase grating fabrication using direct laser writing for generating a two-dimensional focal spot array

Yi Huang[1,3], Minglong Li[1,3], Pu Tu[1], Haodong Zhu[1], Junyu Xia[1], Guangqiang He[2], ZhenYu Yang[1] and Ming Zhao[1,∗]

[1] School of Optical and Electronic Information, Wuhan National Laboratory for Optoelectronics, Huazhong University of Science and Technology, Wuhan 430074, People's Republic of China

[2] State Key Laboratory of Advanced Optical Communication Systems and Networks, Department of Electronic Engineering, Shanghai Jiao Tong University, Shanghai 200240, People's Republic of China

E-mail: zhaoming@hust.edu.cn

Received 15 December 2021, revised 1 March 2022

Accepted for publication 15 March 2022

Published 1 April 2022

Abstract

As a beam splitter, multi-value phase grating (MVPG) has a higher diffraction efficiency than the traditional Damman grating (DG) due to its increased number of phase values within one period of the grating. In this paper, two MVPGs are numerically designed within a 120 μm $\times$ 120 μm area, which generate 4 * 4 and 5 * 5 focal spot arrays in the far field. Both gratings are fabricated by direct laser writing (DLW) technology. Their diffraction efficiencies reach 68.58% and 63.4%, respectively. To compare, DGs with the same size and focal spot arrays are designed and fabricated, whose diffraction efficiencies are tested to be 29.55% and 35.04%, respectively. The results demonstrate the better optical properties of multi-value phase gratings and the capability of DLW in three-dimensional nano-scale diffractive optical element fabrication.

Keywords: multi-value phase grating, diffractive optical element, direct laser writing, focus spot array, diffraction efficiency

(Some figures may appear in colour only in the online journal)

1. Introduction

Diffractive optical element (DOE) is a device made by transparent materials with complex morphology, which can achieve many different optical functions by designing corresponding surface profiles through the diffractive optical theory [1–4]. One application of DOE is a beam splitter, which is widely used in parallel micro-processing, creating 3D spot arrays, optical vortex, multiple imaging, and communication multiplexing [5–13]. Through different surface designs, the beam splitter can either generate multiple spots at different focal depths or a spot array on the same focal plane from a single collimated and coherent beam. The traditional beam splitter utilizes Damman grating (DG) [14–19], which is a typical binary phase grating and has only two phase values, i.e. 0 and π. The binary phase design simplifies the fabrication process, but also limits its theoretical diffraction efficiency. To increase the diffraction efficiency, multi-value phase grating (MVPG) [20–22] is proposed, which has more phase values within one period of the grating.

One method to implement a beam splitter is to use a spatial light modulator (SLM). A focal spots array with high uniformity and high diffraction efficiency can be generated by obtaining the phase hologram through the corresponding algorithm and loading it on the SLM [23]. The SLM is very flexible due to its programmability and its phase hologram can be easily changed, and researchers have already used SLM

[3] Authors contributed equally to this work.

∗ Author to whom any correspondence should be addressed.

to create a focal spots array and applied it to parallel laser processing [24]. However, due to the high cost and complex optical path of the SLM, it is not conducive to integration and large-scale commercial applications. Therefore, it is necessary to develop some fabrication methods to manufacture the micro-nano beam splitter.

Traditional fabrication methods usually rely on photomasks and require multiple lithographic steps and etching processes, such as in electron beam etching [25], focused ion beam etching [26], grayscale lithography [27] and so on. Thus they are complicated, costly and difficult to deal with complex and versatile surface profiles. To solve these problems, we use a maskless 3D lithography technology based on two-photon polymerization (TPP), i.e. direct laser writing (DLW). Due to its low cost, high precision and high flexibility, the DLW has been widely used in the fabrication of various micro-optical components [28–30].

In this paper, we design and optimize four MVPGs with different focal spot arrays. We fabricate two of them with 4 * 4 and 5 * 5 focal spot arrays by DLW. The diffraction efficiency is 68.58% and 63.4% respectively, and the uniformity of spot intensity is 96.34% and 95.17%. In comparison, DGs with focal spot arrays of 4 * 4 and 5 * 5 are also fabricated by DLW. The diffraction efficiency is 29.55% and 35.04% respectively, and the uniformity of spot intensity is 74.66% and 71.02%. The results demonstrate that MVPG has better optical performances than the traditional DG.

2. Design of MVPG

Figures 1(a) and (b) show the phase distribution of DG and MVPG, respectively. A period of DG consists of only two phase values with different distribution widths, while a period of MVPG has multiple different phase values with the same distribution width. The transfer function of one-dimensional MVPG can be expressed as equation (1) [21]:

$$T(x) = \mathrm{comb}(x) \otimes \sum_{n=1}^{N} t_n(x) \tag{1}$$

where the symbol '⊗' denotes the convolution operator, the t_n represents the transmittance function of one-dimensional MVPG which can be written as equation (2):

$$t_n(x) = rect\left(\frac{x-(2n-1)/2N}{1/N}\right)\exp(i\varphi_n) \tag{2}$$

where one period is evenly divided into N equal parts and the φ_n determines the phase distribution of the MVPG. The Fourier transform of the t_n can be expressed as equation (3):

$$\Gamma\{t_n(x)\} = \frac{i}{2\pi v}\{\exp(-i2\pi vn) - \exp[-i2\pi v(n-1)]\} \times \exp(i\varphi_n) \tag{3}$$

where v represents the spatial frequency. The corresponding Fourier coefficients A_j can be written as equation (4):

$$A_j = \begin{cases} \frac{1}{N}\sum_{n=1}^{N}\exp(i\varphi_n), & j=0 \\ \frac{i}{2j\pi}\sum_{n=1}^{N}\left[\exp(-i2j\pi\frac{n}{N}) - \exp\left(-i2j\pi\frac{n-1}{N}\right)\right]\exp(\mathrm{i}\varphi_n), & j\neq 0 \end{cases} \tag{4}$$

where j is the diffraction order. The diffraction efficiency of MVPG is defined as equation (5):

$$\eta = \sum_{j}^{\beta} I_j = \sum_{j}^{\beta} A_j \cdot A_j^* \tag{5}$$

where I_j is the intensity of the jth diffraction order, β is the number of focal spot, and the symbol '*' represents complex conjugate. The uniformity of the focal spot can be defined as equation (6):

$$\psi = 1 - \frac{\max(I_j) - \min(I_j)}{\max(I_j) + \min(I_j)}. \tag{6}$$

The simulated annealing algorithm is used to optimize the one-dimensional MVPG and the optimization evaluation function is defined as equation (7):

$$\phi = \frac{\sum_{j=1}^{\beta}(I_j - I_{\mathrm{av}})^2}{\sum_{j=1}^{\beta} I_j} \tag{7}$$

where I_{av} can be expressed as equation (8):

$$I_{\mathrm{av}} = \frac{1}{\beta}\left(\sum_{j=1}^{\beta} I_j\right). \tag{8}$$

When the value of ϕ is smaller, the diffraction efficiency and uniformity of the MVPG will be higher, which represents that the optimization result is better. Through the optimized design of the simulated annealing algorithm, we can obtain the optimal phase number N and phase values φ_n within one period of the MVPG, in order to maximize the diffraction efficiency and uniformity of the MVPG. Table 1 shows the

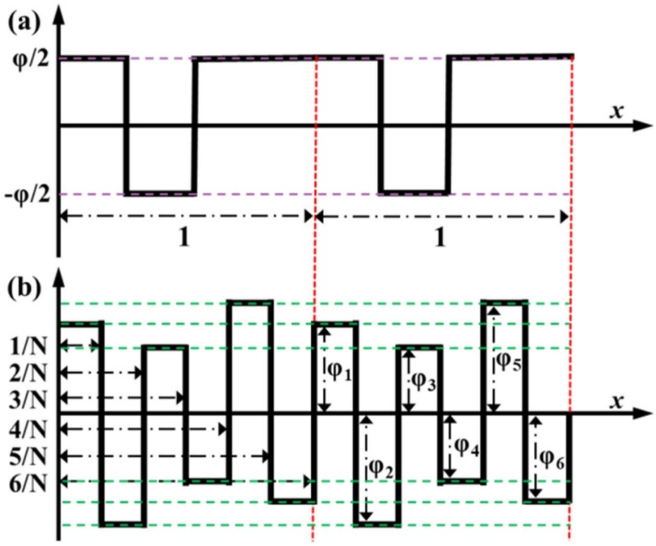

Figure 1. Phase distribution of two gratings. (a) DG with binary phase values. (b) MVPG with six phase values.

Table 1. Optimization results.

β	N	$\varphi_n(\pi)$	η	Ψ
1 * 2	4	0 0 1 1	81.10%	>99%
1 * 3	3	0.71 1.97 1.97	76.4%	>99%
1 * 4	6	0.05 0.53 0.05 1.05 1.53 1.05	85.80%	>99%
1 * 5	4	0.42 0.76 1.69 0.76	84.30%	>99%

optimization results of one-dimensional MVPG with focal spot arrays of 1 * 2, 1 * 3, 1 * 4 and 1 * 5.

The MVPG can be divided into odd type and even type according to the number of focal spots. For the odd type MVPG, each unit in the period can have its own independent phase value. For the even type MVPG, it has a half-period inversion structure, and the phase of the second half period is the π-phase inversion of the first half of the phase distribution. Because the grating structure of the even type MVPG eliminates the sensitivity of zero-order diffracted light to manufacturing errors, the even type MVPG has a higher spot uniformity than odd type MVPG. In table 1, we can see that the diffraction efficiency of one-dimensional optimized MVPG is more than 75% when the spot uniformity is maintained at 99%. By adjusting N and φ_n, the theoretical diffraction efficiency of one-dimensional MVPG with 1 * 4 and 1 * 5 focal spot arrays can reach 85.8% and 84.30%, respectively. After optimization, the phase distributions of two one-dimensional MVPGs are shown in figures 2(a) and (b). By using MATLAB numerical simulation calculation, the simulation results of focal spot arrays and the uniformity of spot intensity of two one-dimensional MVPGs are obtained, as shown in figures 2(c)–(f). Obviously, the optimized one-dimensional MVPG can generate a one-dimensional focal spot array with high uniformity and high diffraction efficiency.

Without any new additional principle or theory, one-dimensional MVPG can be reasonably extended to two-dimensional MVPG. The two-dimensional MVPG can be regarded as the superposition of two orthogonal one-dimensional MVPGs. Figures 3(a) and (b) show the phase distribution of two-dimensional MVPG with 4 * 4 and 5 * 5 focal spot arrays. The grating sizes are 120 μm × 120 μm. Also by using MATLAB numerical simulation calculation, the simulation results of focal spot arrays and the uniformity of spot intensity of two two-dimensional MVPGs are obtained, as shown in figures 3(c)–(f). The simulation results show that the two-dimensional MVPG can generate a two-dimensional focal spot array with high diffraction efficiency and high uniformity. In the next section, we will use DLW technology to fabricate these two two-dimensional MVPGs, and experimentally demonstrate their optical performance.

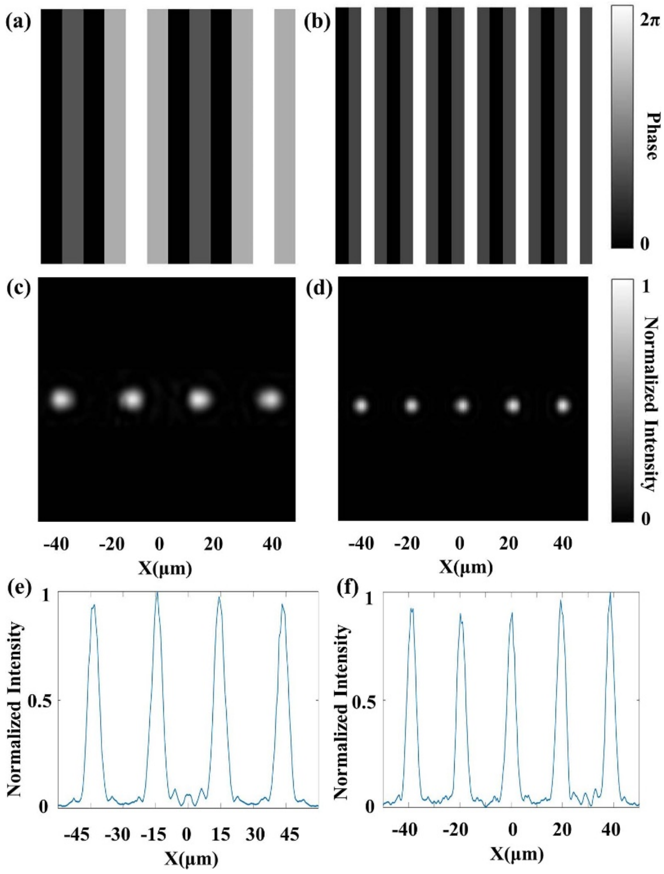

Figure 2. (a) and (b) When the number of focal spots are 1 * 4 and 1 * 5, the phase distribution of two one-dimensional MVPGs; (c) and (d) The spot array generated by two one-dimensional MVPGs simulation; (e) and (f) Intensity distribution of spots along lines X.

3. Manufacture of MVPG

The height of each unit of the MVPG can be calculated by equation (9):

$$d = \frac{\varphi}{k(n_1 - n_0)} \tag{9}$$

where n_1 and n_0 are the refractive indexes of the exposure material and the air at the wavelength of the incident light,

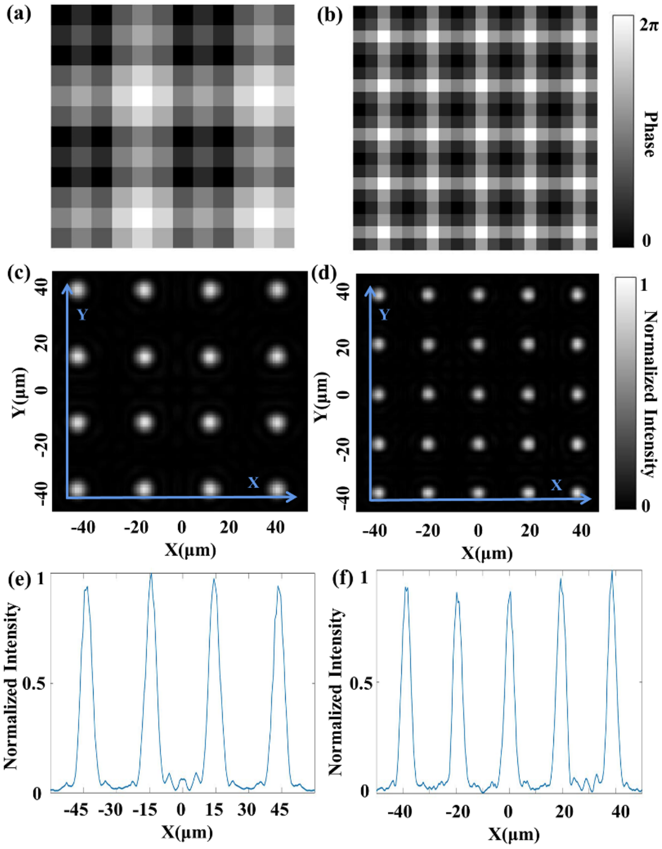

Figure 3. (a) and (b) When the number of focal spots are 4 * 4 and 5 * 5, the two-dimensional phase distribution of MVPG; (c) and (d) The spot array generated by MVPG simulation; (e) and (f) Intensity distribution of spots along lines X.

respectively; φ is the designed phase value of the corresponding unit; k is the wave number of the incident light. We use 1550 nm incident light, and the refractive indexes of IP-dip (Nanoscribe GmbH) photoresist and air at 1550 nm wavelength are 1.53 and 1.00, respectively. In order to ensure that the height of each unit is consistent with the theoretical value, a substrate with a height of 2 μm is prepared, whose surface serves as the zero-reference plane. In order to improve the surface flatness within the unit, both X and Y directions are scanned once separately when filling each unit. Meanwhile, certain compensation processing is added to the direct writing scanning path to ensure the accuracy of the direct writing structure.

Figure 4 shows the schematic diagram of the DLW system, which is composed of the femtosecond fiber laser (Menlo Systems GmbH, C-Fiber 780) with 100 MHz repetition rate, 100 fs pulse width and 780 nm center wavelength. The acousto-optical modulator (Gooch Housego, AOMO 3080–122) is used to control the femtosecond fiber laser power and a 60× oil lens (Nikon, NA 1.4) is used to focus the femtosecond laser beam. A three-dimensional piezoelectric displacement platform (Physik Instrumente, P-563.3 CD) and a two-dimensional galvanometer scanner (Scanlab, Intelliscan III 10) are used to scan the laser beam in a predetermined path in the process of exposures.

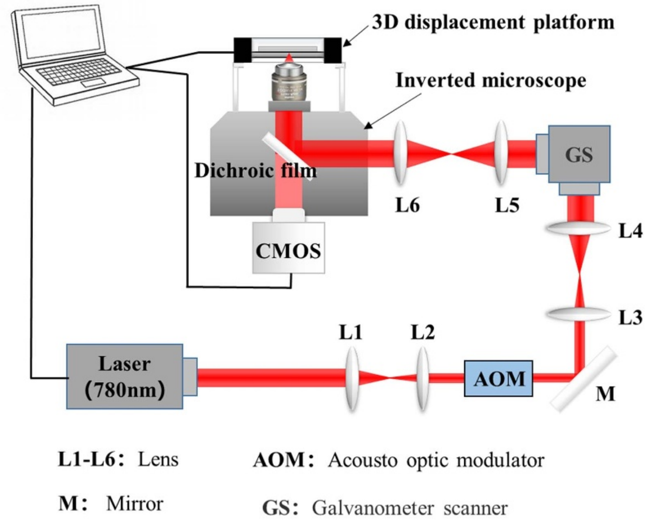

Figure 4. The schematic diagram of the DLW system.

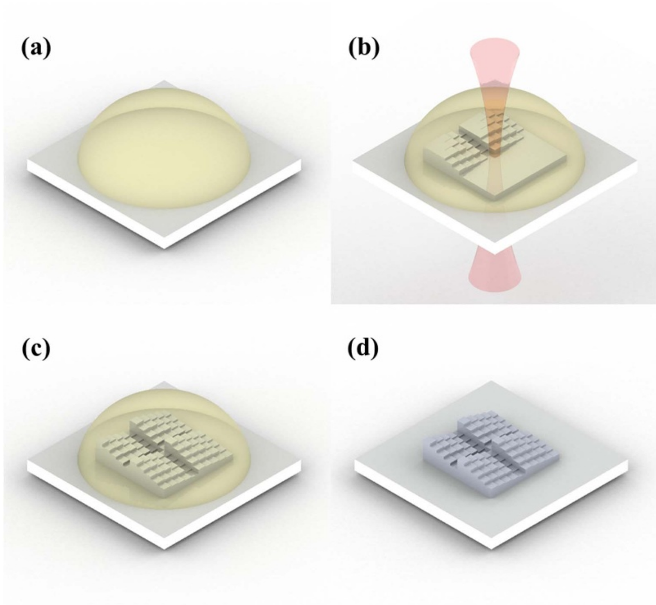

Figure 5. The schematic diagram of the workflow in DLW lithography. (a) Photoresist on the glass slide. (b) Exposure with the focused laser beam. (c) Exposure complete, the grating structure embedded in the unexposed photoresist. (d) After dissolving the unexposed photoresist, leaving a solid grating skeleton.

The schematic diagram of the workflow in DLW lithography as shown in figure 5. The exposure material IP-dip can be directly dropped on the glass slide without spin coating and baking. During the fabrication process, the laser power is set to 30 mW and the laser is scanned line by line in the IP-dip photoresist, which the scanning speed is set to 200 mm s^{-1} and the scanning resolution is set to 0.15 μm. When the fabrication is completed, the glass slide is immersed in the developer (Propylene Glycol Methyl Ether Acetate, PGMEA) for 35 min to dissolve the unexposed photoresist, leaving a solid grating skeleton.

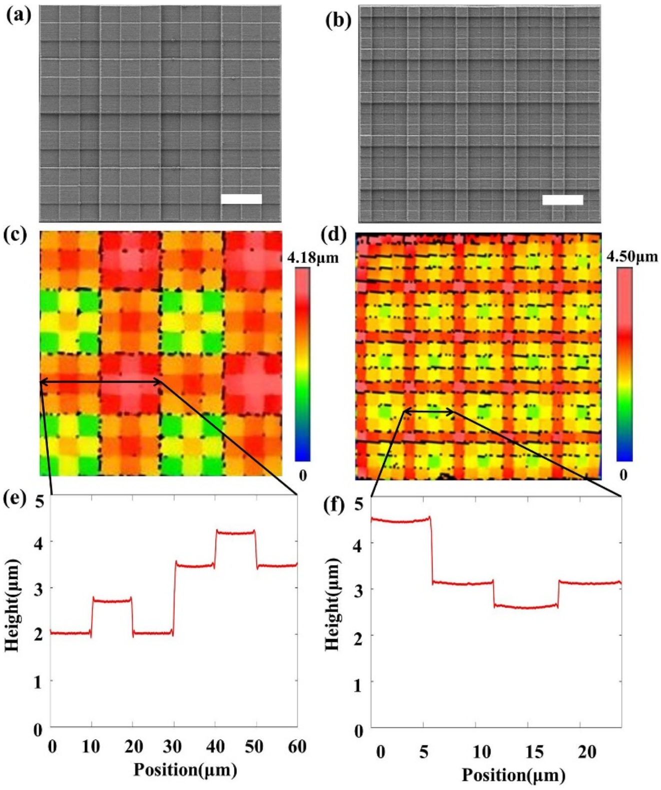

Figure 6. (a) and (b) show the structures of these two MVPGs using a scanning electron microscope, respectively. The scale bar is 20 μm. (c) and (d) 3D profile image of two MVPGs using a profiler. (e) and (f) height distribution curve of a certain part of MVPG in one period.

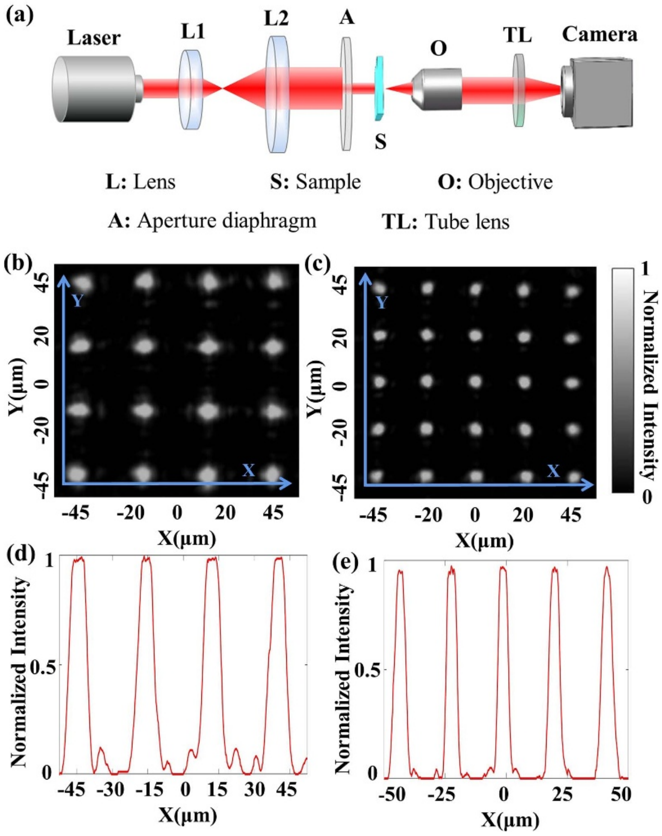

Figure 7. (a) Experimental system for measuring the spot array produced by MVPG; (b) and (c) show the diffraction pattern of the MVPG with 4 * 4 and 5 * 5 focal spot arrays measured by experiment, respectively. (d) and (e) intensity distribution of spots along X.

Figures 6(a) and (b) show the structures of these two MVPGs with different focal spot arrays under a scanning electron microscope (Carl Zeiss, GeminiSEM 300), respectively. The surface of two MVPGs is smooth and the size of each unit is uniform. Figures 6(c) and (d) show 3D profile image of two MVPGs using a profiler (ZYGO, New View 7300). Figures 6(e) and (f) show the one-dimensional height profile as indicated by the black arrow in figures 6(c) and (d). The measured values are consistent with the theoretical design values, and the fabrication error is within 3%.

4. Optical performance of MVPG

In order to observe the diffraction pattern of the MVPG, we set up a test system, as shown in figure 7(a). The 1550 nm laser is expanded through lenses L1 and L2, reaches the MVPG sample surface after going through a small aperture with 100 μms diameter. The imaging system uses an objective lens (O, Olympus, 20×) and a tube lens (TL, focal length 160 mm) to magnify the focal spot array on the MVPG focal plane onto the CCD sensor (Xenics, Bobcat-320, pixel size 20 μm × 20 μm). Figures 7(b) and (c) show the diffraction pattern of the MVPG with 4 * 4 and 5 * 5 focal spot arrays. Next, we will measure and calculate the diffraction efficiency of the MVPG. Since we are more concerned about the focusing ability of light passing through the MVPG, we ignore the Fresnel reflection loss and the absorption loss. The diffraction efficiency in the paper is defined as the ratio of the focal spot energy to the total transmitted energy, which is a concept of relative diffraction efficiency. The measured diffraction efficiencies of the two MVPGs are 68.58% and 63.4%. The experimental diffraction efficiency is lower than the simulation due to limited fabrication accuracy and measurement errors. In addition, they have a slight influence on the uniformity of the spot intensity, which is another criterion for evaluating MVPG. The uniformity curve of the spot intensity is shown in figures 7(d) and (e), and the uniformity is 96.34% and 95.17%, respectively. Therefore, the uniformity of the spot intensity of the MVPG is close to the simulation values.

5. Optical properties of DG

For comparison, we designed two DGs with 4 * 4 and 5 * 5 focal spot arrays within the same 120 μm × 120 μm area using the method from Morrison *et al* [31], Zhou and Liu [32] and Chen *et al* [33]. The grating phase distribution is shown in figures 8(a) and (b). The DGs are also fabricated by DLW. figures 8(c) and (d) show the structures of these two

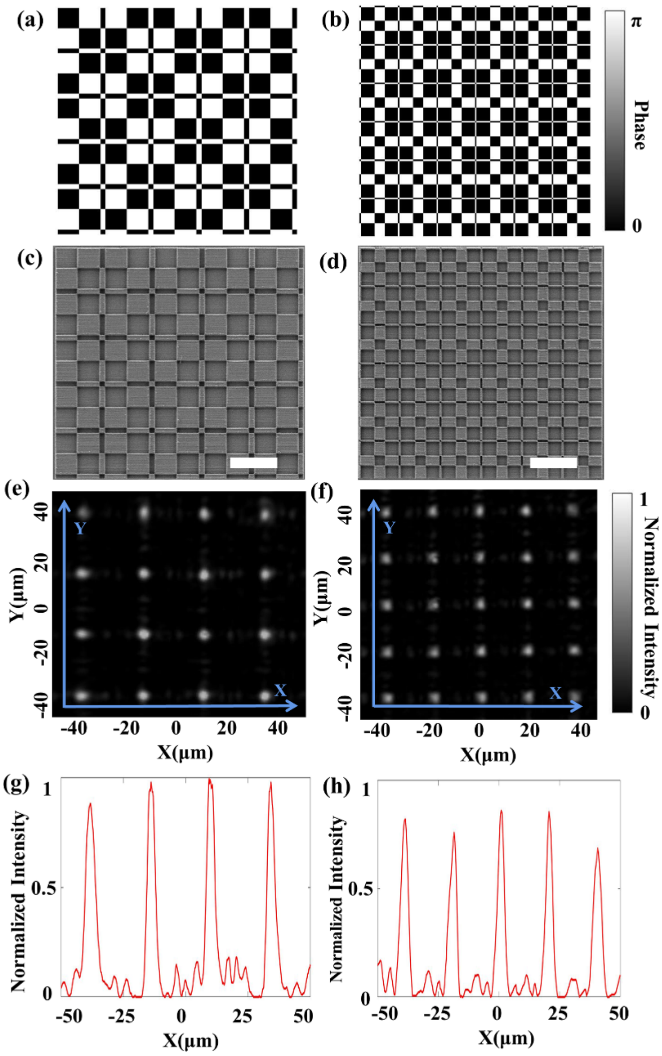

Figure 8. (a) and (b) show the phase distribution diagram of two DGs. (c) and (d) show the structures of these two DGs using a scanning electron microscope, respectively. The scale bar is 20 μm. (e) and (f) show the diffraction pattern of the DG with 4 * 4 and 5 * 5 focal spot arrays measured by experiment, respectively. (g) and (h) intensity distribution of spots along X.

DGs under a scanning electron microscope. Figures 8(e)–(h) show the focal spot arrays and spot intensity uniformity curve of DG. It is calculated that the diffraction efficiency is 29.55% and 35.04%, and the spot uniformity is 74.66% and 71.02%, respectively. The results demonstrate that the MVPG has better optical performance.

6. Summary

In conclusion, we successfully fabricated two different MVPGs and DGs by using DLW, all of which are 120 μm $\times$ 120 μm in size, and can generate either 4 * 4 or 5 * 5 focal spot arrays in the far field. By measuring the far-field intensity distribution of the MVPG on the focal plane, it is shown that the MVPG can realize the function of light splitting. Table 2 lists the optical performance parameters of MVPG and DG obtained in the experiment. The results demonstrate the better optical performance of MVPG over DG and the capability of DLW in the three-dimensional DOEs fabrication. Furthermore, our gratings can be manufactured in minutes and cost only a few dollars. Compared with commercial gratings, our gratings have advantages in manufacturing time and cost. Therefore, the DLW-based maskless lithography provides the possibility for many practical large-scale commercial applications, such as creating 3D spot arrays, multi beam laser parallel processing, multi focus and multi photon microscopic imaging and other fields.

Table 2. The optical performance parameters of MVPG and DG.

	η		Ψ	
β	DG	MVPG	DG	MVPG
4 * 4	29.55%	68.58%	74.66%	96.34%
5 * 5	35.04%	63.4%	71.02%	95.17%

Data availability statement

All data that support the findings of this study are included within the article (and any supplementary files).

Funding

This work is supported by the Natural Science Foundation of China (Nos. 62075073, 62135004 and 62075129), the Fundamental Research Funds for the Central Universities (No. 2019kfyXKJC038), State Key Laboratory of Advanced Optical Communication Systems and Networks, Shanghai Jiao Tong University (No. 2021GZKF007), and Key R & D project of Hubei Province (No. 2021BAA003).

Acknowledgments

We would like to thank Dr Shuwen Wei for the revisions and the suggestions on this manuscript.

Conflict of interest

The authors declare no conflicts of interest

ORCID iDs

Yi Huang https://orcid.org/0000-0002-5550-8245
Guangqiang He https://orcid.org/0000-0001-9017-4159

References

[1] Wang H, Liu Y, Ruan Q, Liu H, Ng R J H, Tan Y S, Wang H, Li Y, Qiu C W and Yang J K W 2019 Off-axis holography with uniform illumination via 3D printed diffractive optical elements *Adv. Opt. Mater.* **7** 1900068

[2] Wildi T, Kiss M and Quack N 2020 Diffractive optical elements in single crystal diamond *Opt. Lett.* **45** 3458–61

[3] Xiong Z, Puskal K and Pranav S 2021 Hydrogel-based diffractive optical elements (hDOEs) using rapid digital photopatterning *Adv. Opt. Mater.* **9** 2001217

[4] Mu T, Chen Z, Pacheco S, Wu R, Zhang C and Liang R 2016 Generation of a controllable multifocal array from a modulated azimuthally polarized beam *Opt. Lett.* **41** 261–4

[5] Kuang Z, Perrie W, Liu D, Edwardson S P, Jiang Y, Fearon E, Watkins K G and Dearden G 2013 Ultrafast laser parallel microprocessing using high uniformity binary Dammann grating generated beam array *Appl. Surf. Sci.* **273** 101–6

[6] Davis J A, Moreno I, Martínez J L, Hernandez T J and Cottrell D M 2011 Creating three-dimensional lattice patterns using programmable Dammann gratings *Appl. Opt.* **50** 3653–7

[7] Yu J, Zhou C, Jia W, Cao W, Wang S, Ma J and Cao H 2012 Three-dimensional Dammann array *Appl. Opt.* **51** 1619–30

[8] Yu J, Miao C, Wu J and Zhou C 2020 Circular Dammann gratings for enhanced control of the ring profile of perfect optical vortices *Photon. Res.* **8** 648–58

[9] Lei T *et al* 2015 Massive individual orbital angular momentum channels for multiplexing enabled by Dammann gratings *Light Sci. Appl.* **4** 2095–5545

[10] Zhu Y, Zhang C, Gong Y, Zhao W, Bai J and Wang K 2021 Realization of flexible and parallel laser direct writing by multifocal spot modulation *Opt. Express* **29** 8698–709

[11] Lin H, Jia B and Gu M 2011 Dynamic generation of Debye diffraction-limited multifocal arrays for direct laser printing nanofabrication *Opt. Lett.* **36** 406–8

[12] Weng X, Wang L, Yan W and Qu J 2019 Tunable plasmonic focus array generated by Dammann grating in tightly focusing system *J. Opt.* **21** 015001

[13] Zhang H, Fu C, Fang J, Lei T, Zhang Y and Yuan X 2020 Cylindrical vector beams demultiplexing optical communication based on spin-dependent vortex Dammann grating *Appl. Opt.* **59** 11041–5

[14] Wang H, Wang H, Zhang W and Yang J K W 2020 Toward near-perfect diffractive optical elements via nanoscale 3D printing *ACS Nano* **14** 10452–61

[15] Li Q K, Chen Q D, Niu L G, Yu Y H, Wang L, Sun Y L and Sun H B 2016 Sapphire-based Dammann gratings for UV beam splitting *IEEE Photon. J.* **8** 2500208

[16] Zheng Q, Zhou J, Chen Q, Lei L, Wen K and Hu Y 2019 Rapid prototyping of a Dammann grating in DMD-based maskless lithography *IEEE Photon. J.* **11** 2400410

[17] Zhang H, Zhang Z, Song X, Zhao R, Jia D and Liu T 2021 Tunable multi-wavelength optofluidic Dammann grating with beam splitting property *Opt. Express* **29** 33414–23

[18] Zeng T, Chang C, Chen Z, Wang H T and Ding J 2018 Three-dimensional vectorial multifocal arrays created by pseudo-period encoding *J. Opt.* **20** 065605

[19] Weng X, Du L, Shi P and Yuan X 2017 Tunable optical cage array generated by Dammann vector beam *Opt. Express* **25** 9039–48

[20] Walker S J and Jahns J 1990 Array generation with multilevel phase gratings *J. Opt. Soc. Am.* A **7** 1509

[21] Zhu L, Sun M, Zhu M, Chen J, Gao X, Ma W and Zhang D 2014 Three-dimensional shape-controllable focal spot array created by focusing vortex beams modulated by multi-value pure-phase grating *Opt. Express* **22** 21354–67

[22] Ghebjagh S G, Fischer D and Sinzinger S 2019 Multifocal multi-value phase zone plate for 3D focusing *Appl. Opt.* **58** 8943–9

[23] Mikhaylova D, Zhou B F, Kiedrowski T, Mikut R and Lasagni A F 2019 High accuracy beam splitting using spatial light modulator combined with machine learning algorithms *Opt. Lasers Eng.* **121** 227–35

[24] Yang L, El-Tamer A, Hinze U, Li J, Hu Y, Huang W, Chu J and Chichkoy B N 2015 Parallel direct laser writing of micro-optical and photonic structures using spatial light modulator *Opt. Lasers Eng.* **70** 26–32

[25] Grigaliūnas V, Lazauskas A, Jucius D, Viržonis D, Abakevičienė B, Smetona S and Tamulevičius S 2016 Microlens fabrication by 3D electron beam lithography combined with thermal reflow technique *Microelectron. Eng.* **164** 23–29

[26] Liu Z, Abbasi H N, Zhu T F, Wang Y F, Fu J, Wen F, Wang W, Fan S, Wang K and Wang H X 2019 Fabrication of micro lens array on diamond surface *AIP Adv.* **9** 125218

[27] Wu M H, Park C and Whitesides G M 2002 Fabrication of arrays of microlenses with controlled profiles using gray-scale microlens projection photolithography *Langmuir* **18** 9312–8

[28] Huang Y, Qin Y, Tu P, Zhang Q, Zhao M and Yang Z Y 2020 High fill factor microlens array fabrication using direct laser writing and its application in wavefront detection *Opt. Lett.* **45** 4460–3

[29] Zhang D, Wei H, Hu H and Krishnaswamy S 2020 Highly sensitive magnetic field microsensor based on direct laser writing of fiber-tip optofluidic Fabry–Pérot cavity *APL Photon.* **5** 076112

[30] Cai Z *et al* 2020 Dynamic airy imaging through high-efficiency broadband phase microelements by femtosecond laser direct writing *Photon. Res.* **8** 875–83

[31] Morrison R L, Walker S L and Cloonan T J 1993 Beam array generation and holographic interconnections in a free-space optical switching network *Appl. Opt.* **32** 2512–8

[32] Zhou C and Liu L 1995 Numerical study of Dammann array illuminators *Appl. Opt.* **34** 5961–9

[33] Chen Q D, Lin X F, Niu L G, Wu D, Wang W Q and Sun H B 2008 Dammann gratings as integratable micro-optical elements created by laser micronanofabrication via two-photon photopolymerization *Opt. Lett.* **33** 2559–61